Theoretical ONIOM2 Study on Pyridine Adsorption in the Channels and Intersection of ZSM-5

Shuping Yuan,[†] Wei Shi,[‡] Bingrui Li,[‡] Jianguo Wang,*[,†] Haijun Jiao,[†,§] and Yong-Wang Li[†]

State Key Laboratory of Coal Conversion, Institute of Coal Chemistry, Chinese Academy of Sciences, P.O. Box 165, Taiyuan 030001, P. R. China, College of Chemistry and Chemical Engineering, Lanzhou University, Lanzhou 730000, P. R. China, and Leibniz-Institut für Organische Katalyse an der Universität Rostock, Buchbinderstrasse 5-6, 18055 Rostock, Germany

Received: September 6, 2004; In Final Form: December 18, 2004

The structures of the acid sites in the channels and intersections of H−, Li−, and Na−ZSM-5 (ZSM = zeolite socony mobil) and their interactions with pyridine molecule have been computed by using three corresponding models containing 22 tetrahedral sites. The calculated adsorption energies of pyridine in the intersection regions of H−, Li−, and Na−ZSM-5 are 197.0, 172.5, and 122.3 kJ/mol, respectively, in good agreement with the respective experimental values of 200 ± 5, 155−195, and 120 kJ/mol, while those in the straight and sinusoidal channels are much smaller (157.9 and 127.6, 152.2 and 149.4, and 150.4 and 109.9 kJ/mol, respectively). These indicate that the most probable adsorption site for pyridine in ZSM-5 is the acidic site located in the intersection region. The structural parameters of the adsorption complexes show that the acidic proton in the three models of H−ZSM-5 has been transferred to the nitrogen of pyridine, while in alkali cation-exchanged ZSM-5, the coordination of the alkali cation to the nitrogen atom of pyridine dominates the overall interaction. In addition, the adsorption complexes were further stabilized by the long-range electrostatic interaction between the positively charged pyridine hydrogen atoms and the negatively charged lattice oxygen atoms of the zeolite framework. In the intersection regions of H−, Li−, and Na−ZSM-5, the coordination energy of the charge-compensating cation to the pyridine nitrogen amounts to 58, 60, and 68% of the total adsorption energy, respectively, while another 42, 40, and 32%, respectively, is due to long-range electrostatic interactions. This indicates that the zeolite lattice framework surrounding the adsorption site has important contributions to the adsorption energy of the pyridine molecule.

1. Introduction

Zeolites are important shape-selective acidic catalysts in petroleum reforming, synfuel production, petrochemical production, and the synthesis of fine chemicals. Channels and cavities of their framework provide both high surface area and shape selectivity as catalysts, while bridging hydroxyl groups introduced by the substitution of Si by Al or other trivalent metal atoms are responsible for their Brønsted acidity. In addition, because of the specific balance of acidic and basic functions, alkali-metal cation-exchanged zeolites have been found to be potential catalysts in reactions such as the side-chain alkylation of toluene[1] and condensation reactions[2] or to be selective sorbents in separation technologies.[3]

A better understanding of the strength of the acidic centers and their relative positions in zeolite structures is important for the successful description of the catalytic and adsorption properties of proton and alkali-metal cation-exchanged zeolites. Experimentally, various methods have been employed to locate the positions of the Lewis and Brønsted acidic sites in zeolites and their interaction with probe molecules. Ammonia and pyridine are the most frequently used probe molecules for the acid strength of zeolites because it is assumed that the acid strength can be inferred from the heat of adsorption for these simple base molecules. For instance, pyridine has been used as an indicator of the acidity of zeolite in infrared,[4] temperature-programmed desorption,[5] X-ray photoelectron spectroscopy,[6] and NMR[7] experiments. However, these experiments provide an average picture of zeolite, and detailed information on local structure and reaction mechanisms within zeolite are still elusive. In the past few decades, theoretical methods have become a useful, complementary tool to experimental techniques to get information pertinent to the local electronic and structural properties of zeolite.

Up until now, numerous theoretical models have been proposed to study the structures and acidic properties of zeolites. The most widely used procedure is small cluster models for describing catalytic active sites of zeolites.[8−10] However, these small models cut from zeolites do not reflect the framework reasonably, on the one hand, and neglect the long-range electrostatic interactions, on the other hand. Periodic ab initio calculation is an alternative approach to overcome this limitation, but zeolites in practical processes usually have hundreds of atoms per unit cell, and this large size makes the use of periodic ab initio methods too computationally expensive or impossible. The development of embedding cluster methods and a combination of quantum and molecular mechanics (QM/MM) hybrid methods are effective ways to describe the zeolite framework at a reasonable computational cost with rather precise results.[11] The ONIOM method, developed by Morokuma and co-workers and implemented in the Gaussian 03 program, is a more general

* Author to whom correspondence should be sent. E-mail: iccjgw@sxicc.ac.cn.
[†] Chinese Academy of Sciences.
[‡] Lanzhou University.
[§] Universität Rostock.

10.1021/jp045979f CCC: $30.25
Published on Web 03/01/2005

QM/MM or QM/QM method[12] in which a high-level QM method is applied only to the sites of interest (adsorbates, reactants, and catalytic active sites) and a low-level QM or MM method is applied for the rest of the zeolite framework. It has the advantages of high QM accuracy and high MM efficiency simultaneously.

Many calculations have been done for the adsorption of pyridine in zeolites.[13] Because of limited computer resources in the past, the structure of zeolite was modeled by small clusters, in which only the acidic site and its nearest neighbors are included. These small clusters can give a good description of the adsorption of small molecules such as CO,[14] NH_3,[9,10,15] CH_3OH,[16] and H_2O[17] in zeolite's acidic sites. However, for larger molecules such as pyridine, with dimensions close to the diameters of the straight channels, ca. 5.4 × 5.6 Å, and the sinusoidal channels, ca. 5.1 × 5.4 Å, of ZSM-5, the heats of adsorption are related both to the intrinsic acidity of the acidic site and to the interaction between the deprotonated zeolites and the protonated base. Therefore, small clusters, which neglect the effect of the framework, can significantly change the structure and energies of the system and lead to rather smaller ΔE_{ads} values (ΔE_{ads} = adsorption energy) as compared to those of the experiments.

In recent years, ONIOM methods have been frequently used to study the extended systems such as enzymes,[18] metal surfaces,[19] and zeolite properties.[20] Roggero et al.[21] have successfully used the ONIOM method to model the adsorption of NH_3 at the isolated hydroxyl groups on a highly dehydrated silica surface. It has also been applied successfully to study the catalytic reactions on H−ZSM-5.[22] However, there are no reports on the application of the ONIOM method to the interaction of zeolite acidic sites with pyridine as a probe molecule. In this work, we present ONIOM2 theoretical studies on the local structures of the acidic sites in the straight and sinusoidal channels and the intersections of these two channels for H^+-, Li^+-, and Na^+-exchanged ZSM-5 as well as their interactions with pyridine.

2. Computational Details

2.1. Models. The cluster models are taken from the lattice structure of Na−ZSM-5, in which there are 12 distinct tetrahedral sites (T_x, $x = 1-12$) in the unit cell.[23] Three different clusters containing 22 tetrahedral sites (Figure 1) are used to model the straight and sinusoidal channels and their intersections of ZSM-5, respectively. In these three clusters, an aluminum atom replaces a silicon atom and the resulting negative charge is compensated by H^+, Li^+, or Na^+ to produce H−, Li−, and Na−ZSM-5, respectively. In the clusters of the sinusoidal channel and the intersection region, an Al atom is at the T_{12} site,[24] while in the straight channel, an A1 atom is at the T_7 site.[25] The dangling bonds in these models are replaced by Si−H with a distance of 1.48 Å.

It is necessary to point out that our models have been chosen on the basis of the realistic sizes of the channels and the intersection and also on the basis of our computer power, and the structures have been optimized partially, although the best model should be a real cluster fully optimized at a high correlated level and sufficient basis set. This is because the relaxation of the zeolite framework upon adsorption is rather local around the active site.[20,26] On the other hand, the strain caused by partially optimized structures can be canceled or compensated largely between the clusters and adsorbed clusters for the calculation of ΔE_{ads} values. In addition, we have used 2T, 4T, and 8T models to make sure that our results are reliable and meaningful. Indeed, the very good agreement between theoretical and experimental ΔE_{ads} values reveals the high quality of our model systems, and therefore our results are qualitatively meaningful and quantitatively reliable.

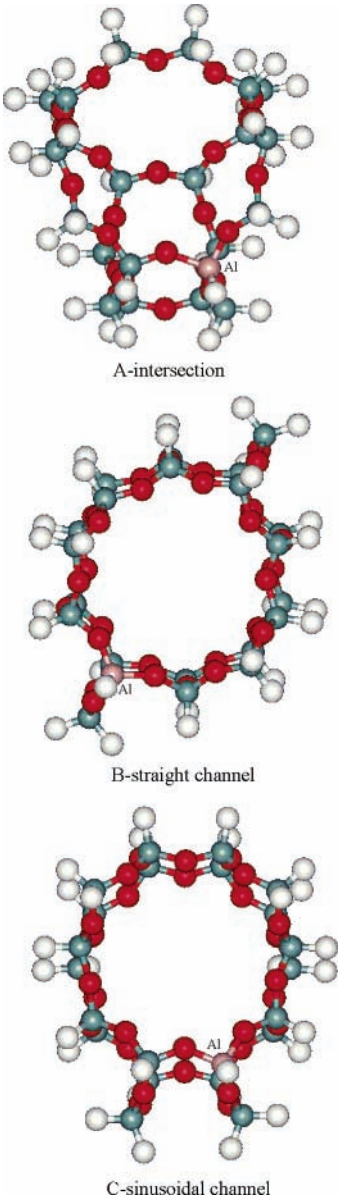

Figure 1. 22T clusters simulating the intersection (A), the straight channel (B), and the sinusoidal channel (C) of ZSM-5.

2.2. Methods. All calculations are performed using the ONIOM2 method in the Gaussian 03 program.[27] In the framework of ONIOM2, the system is divided into two layers and treated at two different levels of theory; that is, the active region is treated more accurately with the B3LYP/6-31G(d,p) density functional method, while interaction in the rest of the clusters is approximated by the HF/3-21G ab initio method. In this work, the 4T model of the ZSM-5 bare cluster forming the high-level layer (shown as ball-and-stick in Figures 2−4) is described at B3LYP/6-31G(d,p). In the adsorption complexes, pyridine is also included in the high-level region. The rest of the cluster forming the low-level layer is described at HF/3-21G. Four linking H atoms between these two layers replace four oxygen atoms in the clusters to avoid the chemically unrealistic model.

What should be mentioned is that density functional methods have limitations for taking the dispersive energy into account.[22]

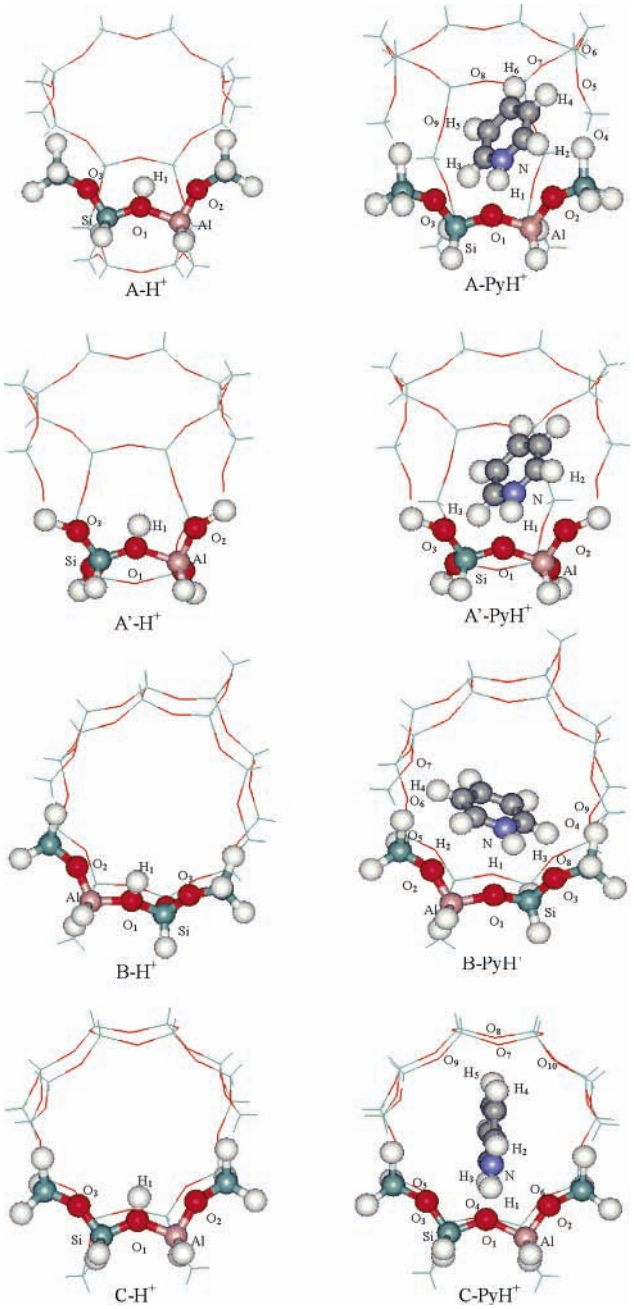

Figure 2. **22/4T** ONIOM2 models (A′−H$^+$, **22/2T**) and their pyridine adsorption complexes in the intersection and channels of H−ZSM-5, in which stick-and-ball structures represents the high layer, while lines represent the low layer: A−H$^+$ (A′−H$^+$)/A−PyH$^+$ (A′−PyH$^+$) for the intersection; B−H$^+$/B−PyH$^+$ for the straight channel; and C−H$^+$/C−PyH$^+$ for the sinusoidal channel.

However, the dispersion forces are a minor component of the ΔE_{ads} values because interactions in the present studied systems are through medium-strength H bonds. Therefore, the B3LYP hybrid functional with the 6-31G(d,p) basis set including a polarization function on hydrogen is expected to predict reasonably accurate interaction energies. The HF/3-21G method used for the low-level layer would overestimate the hydrogen-bonding interaction energies. Thus, the ΔE_{ads} values obtained in this work would be somewhat larger than more accurate theoretical values. In addition, all of the energies reported do not include corrections for zero-point energy because their values would likely be similar for each of the clusters and, thus, would have no influence on conclusions based on the relative energies. Basis-set superposition errors were not calculated because they would be a small factor, of several calories per mole, and a relatively constant energetic offset across the cluster models we compared,[28] and the same is also applicable to the intramolecular dispersion effect for the density functional theory method.[29]

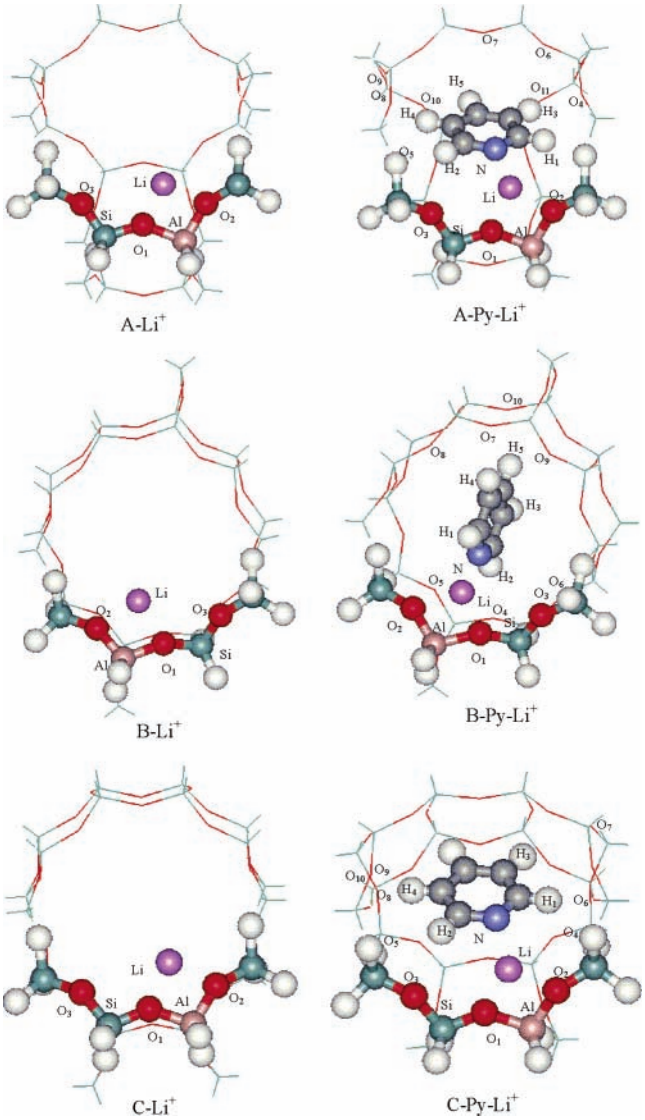

Figure 3. **22/4T** ONIOM2 models and their pyridine adsorption complexes in the intersection and channels of Li−ZSM-5, in which stick-and-ball structures represent the high layer, while lines represent the low layer: A−Li$^+$/A−Py−Li$^+$ for the intersection; B−Li$^+$/B−Py−Li$^+$ for the straight channel; and C−Li$^+$/C−Py−Li$^+$ for the sinusoidal channel.

The clusters representing the framework of ZSM-5 are all partially optimized with the relaxation of the $SiOAlO_3$ moiety and the charge-compensating cation, while the rest of the model is fixed in its bulky position. For the adsorption complexes, pyridine is fully relaxed along with the zeolite framework. The optimized structures are the most stable adsorbed complexes around the acidic center, while adsorption outside the acidic center has not been included.

3. Results and Discussion

3.1. Structures of the Acidic Sites in H−, Li−, and Na−ZSM-5. To give a detailed description of pyridine adsorption in ZSM-5 with a reasonable resource cost, two 22T models representing the intersection region of H−ZSM-5, with the high-layer models being 2T (**22/2T**; Figure 2, A′−H$^+$) and 4T (**22/4T**; Figure 2, A−H$^+$), are used for pyridine adsorption (Figure

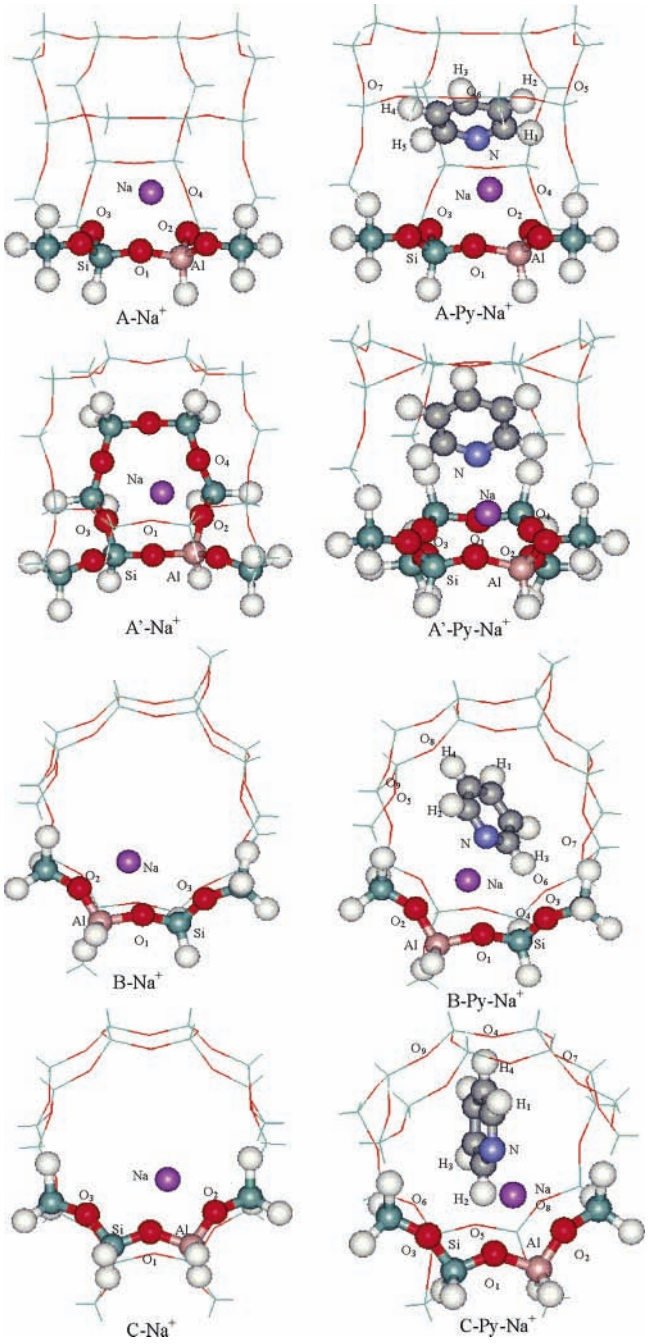

Figure 4. **22/4T** ONIOM2 models (A′−Na^+, **22/8T**) and their pyridine adsorption complexes in the intersection and channels of Na−ZSM-5, in which stick-and-ball structures represent the high layer, while lines represent the low layer: A−Na^+ (A′−Na^+)/A−Py−Na^+ (A′−Py−Na^+) for the intersection; B−Na^+/B−Py−Na^+ for the straight channel; and C−Na^+/C−Py−Na^+ for the sinusoidal channel.

2, A′−PyH^+ and A−PyH^+; PyH^+ = pyridinium ion). From the structural parameters of the acid sites calculated from these two schemes (Table 1), it is shown that the O_1-H_1 bond distance, which reflects the acid strength of the Brønsted site, is not obviously affected by the different selection of the high-level layer. The $Al-O_1$ and $Al-O_2$ bond lengths and the angle between the $Si-O_1$ and $Al-O_1$ bonds ($\alpha_{Al-O1-Si}$) are also hardly affected. However, a difference is observed in the $Al-H_1$ distances of these two models. The R_{Al-H1} value of 2.318 Å for **22/4T** is closer to the NMR experimental value of 2.38 ± 0.04 Å[30] than the value of 2.304 Å for **22/2T**, which indicates that more accurate results can be obtained with **22/4T**. The ΔE_{ads} values in Table 2 show further that **22/4T** is more efficient to describe the acidic sites and their interaction with pyridine; that is, the calculated ΔE_{ads} for **22/4T** is 197.0 kJ/mol, which agrees nicely with the experimental value of 200 ± 5 kJ/mol,[31] while the energy calculated for **22/2T** is only 186.0 kJ/mol. As a result, we used **22/4T** models to finish the remaining calculations and discussion.

TABLE 1: Structural Parameters of the Bare H−ZSM-5 Framework Models[a]

	intersection A′−H^+ (**22/2T**)	intersection A−H^+ (**22/4T**)	straight channel B−H^+ (**22/4T**)	sinusoidal channel C−H^+ (**22/4T**)
R_{Al-O1}	1.907	1.911	1.801	1.759
R_{Al-O2}	1.712	1.717	1.636	1.688
R_{Si-O1}	1.593	1.594	1.657	1.646
R_{O1-H1}	0.979	0.978	0.982	0.977
R_{Al-H1}	2.304	2.318	2.215	2.260
$\alpha_{Si-O1-Al}$	141.0	140.8	152.6	134.6

[a] For the numbering systems, see Figure 2.

TABLE 2: Adsorption Energies (kJ/mol) of Pyridine in the Two Channels and Channel Intersections of H−, Li−, and Na−ZSM-5

	22/4T	small cluster	expt
H−ZSM-5			
intersection (A−PyH^+)	197.0 (186.0)[a]	115.0[b]	
straight channel (B−PyH^+)	127.6	97.4[c]	200 ± 5
sinusoidal channel (C−PyH^+)	157.9	81.7[c]	
Li−ZSM-5			
intersection (A−Py−Li^+)	172.5	104.3[c]	
straight channel (B−Py−Li^+)	149.4	104.2[c]	155−195
sinusoidal channel (C−Py−Li^+)	152.2	112.5[c]	
Na−ZSM-5			
intersection (A−Py−Na^+)	122.3 (112.1)[d]	82.7[e]	
straight channel (B−Py−Na^+)	109.9	78.8[c]	120
sinusoidal channel (C−Py−Na^+)	150.4	100.3[c]	

[a] Calculated from the **22/2T** model of the intersection region of H−ZSM-5. [b] Calculated from the **2T** model, which is cut from the high-level layer of the **22/2T** model of the intersection region of H−ZSM-5. [c] Calculated from the **4T** model, which is cut from the high-level layer of the corresponding **22/4T** models. [d] Calculated from the **22/8T** model of the intersection region of Na−ZSM-5. [e] Calculated from the **8T** model, which is cut from the high-level layer of the **22/8T** model of the intersection region of Na−ZSM-5.

Optimization of the three **22/4T** models representing the intersection and the straight and sinusoidal channels of H−ZSM-5 leads to different fine structures of the Brønsted sites (Table 1). Although the O_1-H_1 distance shows similar results in the three models, the bond angle of $\alpha_{Al-O1-Si}$ shows a significant difference. It was also found that the replacement of Si by Al leads to a larger distortion of the zeolite structure in the intersection region than it does in the two channels, as indicated by the R_{Al-O1} and R_{Al-O2} bond lengths. The smaller R_{Al-O1} distances in the two channels also lead to shorter $Al-H_1$ bonds as compared to those of the intersection model. In addition, large differences in the Al−O bond distances in the intersection and the straight and sinusoidal channels are found (R_{Al-O1} and R_{Al-O2} in Table 1); this is mainly due to the different structural characteristics of these three models. The substitution atom Al can relax much more in the intersection region than it can in the two channels; thus, the Al−O bonds in the intersection model are much longer than those of the two channels. This model has been validated by a good agreement in theoretical and experimental ΔE_{ads} values, as discussed in the previous section.

TABLE 3: Structural Parameters of the Bare Li−ZSM-5 and Na−ZSM-5 22/4T Framework Models[a]

	Li−ZSM-5			Na−ZSM-5		
	intersection	straight channel	sinusoidal channel	intersection[b]	straight channel	sinusoidal channel
R_{Al-O1}	1.785	1.741	1.729	1.752/[1.799]	1.744	1.718
R_{Al-O2}	1.756	1.642	1.689	1.689/[1.712]	1.647	1.685
R_{Si-O1}	1.593	1.606	1.611	1.594/[1.601]	1.596	1.591
$\alpha_{Si-O1-Al}$	140.7	154.2	136.9	142.0/[142.5]	154.3	138.4
R_{X-O1}	1.897	2.002	1.892	2.754/[2.616]	2.345	2.252
R_{X-O2}	1.940	2.012	1.940	2.254/[2.305]	2.316	2.268
R_{Al-X}	2.506	2.441	2.486	2.941/[2.881]	2.867	2.895
R_{X-O3}				2.818/[2.771]		
R_{X-O4}				2.579/[2.744]		

[a] For the numbering systems, see Figures 3 and 4. [b] Values calculated from the **22/8T** model of the intersection region of Na−ZSM-5 are in square brackets.

In H−ZSM-5, the charge-compensating proton is attached to one of the framework oxygen atoms bonded to Al and, thus, forms the bridging hydroxyl group $Al-O_1(H_1)-Si$ in the models of $A-H^+$, $B-H^+$, and $C-H^+$ in Figure 2. In the alkali-metal cation-exchanged ZSM-5, Li^+ and Na^+ are located near the Al and interact with the O_1 and O_2 atoms that are bonded to the Al more or less symmetrically, in both the channels and the intersection for Li^+ (Table 3 and Figure 3, $A-Li^+$, $B-Li^+$, and $C-Li^+$) and only in the channels for Na^+ (Figure 4, $B-Na^+$ and $C-Na^+$), while in the intersection model of Na−ZSM-5, Na^+ has a 4-fold interaction (Figure 4, $A-Na^+$). The symmetric binding between the alkali-metal cation and $[AlO_4^-]$ of the zeolite has been confirmed by an electron spin resonance experiment[32] and theoretical studies.[33,34] In the intersection model of Na−ZSM-5, Na^+ is located above the middle of the six-membered ring and lies at a short distance (2.254−2.818 Å) from four of the oxygen atoms and at a longer distance (3.227−3.792 Å) from the other two oxygen atoms of the ring. The location of Na^+ in a six-membered ring of Faujasite zeolite has been studied by density functional methods by Vayssilov et al.,[35] and they found that, with only one Al in the six-membered ring, Na^+ is almost in the plane of the six-membered ring of Sodalite cages. Considering that interactions of O_3 and O_4 with Na^+ in the intersection model of Na−ZSM-5 (Figure 4, $A-Na^+$) belong to the low-level layer, calculations are carried out on the **22/8T** ONIOM2 model (Figure 4, $A'-Na^+$), with 8T as a high-layer model and the complete six-membered ring included in the high-level layer. It was shown that the optimization of this model leads to results similar to those of the **22/4T** model (Table 3). This indicates that, in the intersection region of ZSM-5, the most stable position for the Na^+ ion is above the six-membered ring, in which Na^+ forms a 4-fold coordination with the framework oxygen.

Compared to those of H−ZSM-5, the interactions of Li^+ and Na^+ with the zeolite framework lead to less perturbation of the atoms around the acidic sites, as indicated by the Al−O and Si−O bond lengths (Table 3). This can be attributed to the electrostatic interaction between the charge-compensating alkali-metal cation and the zeolite framework oxygen, while in H−ZSM-5, the proton forms a covalent bond with the bridging oxygen O_1. Li^+ interacts with two oxygen atoms bonded to Al at distances of 1.892−2.012 Å and Na^+ bonded to two or four oxygen atoms at distances of 2.252−2.818 Å. The Al−Li and Al−Na distances in the intersection model of 2.506 and 2.941 Å, respectively, are close to the values of other theoretical ONIOM studies, in which the Al−Li bond is 2.566 Å and the Al−Na bond is 2.961 Å.[33] It was also found that the Al−Na bond is longer than the Al−Li bond, in agreement with the increasing radius of these two cations (Pauling radius: Li^+, 0.60 Å; Na^+, 0.95 Å[36]). The longest $Al-O_1$ bonds of the intersection models in Li− and Na−ZSM-5 resulted in the longest Al−Li and Al−Na bonds when compared to those of the models of the two channels.

TABLE 4: Structural Parameters of Pyridine Adsorption Complexes in H−ZSM-5 Models[a]

	intersection ($A-PyH^+$)	straight channel ($B-PyH^+$)	sinusoidal channel ($C-PyH^+$)
R_{Al-O1}	1.767	1.801	1.801
R_{Al-O2}	1.737	1.664	1.690
R_{Si-O1}	1.603	1.573	1.632
R_{Al-H1}	2.524	3.654	2.640
$\alpha_{Si-O1-Al}$	141.7	155.0	133.0
R_{N-H1}	1.047	1.019	1.086
R_{O1-H1}	1.763	2.418	1.474
R_{O2-H2}	2.434	2.461	
R_{O3-H3}		2.525	
R_{O2-H1}	2.775		2.533
R_{O3-H1}		2.269	2.742
R_{O4-H2} (R_{O4-H3})	2.428	(2.530)	(2.342)
R_{O5-H4} (R_{O5-H3})	2.936	2.893	(2.830)
R_{O6-H4} (R_{O6-H3})	2.425	2.756	(2.774)
R_{O7-H6} (R_{O7-H4})	2.381	(2.436)	(2.919)
R_{O8-H5} (R_{O8-H3})	2.875	(2.848)	2.213
R_{O8-H6}	2.881		
R_{O9-H5} (R_{O9-H3})	2.657	(2.145)	2.761
R_{O10-H5}			2.679

[a] For the numbering systems, see Figure 2.

3.2. Structure of the Adsorption Complexes of Pyridine in H−, Li−, and Na−ZSM-5. Figures 2−4 and Tables 4 and 5 present the optimized structures and the selected structural parameters of pyridine adsorption complexes on H−, Li−, and Na−ZSM-5. From the configurations of $A-PyH^+$, $B-PyH^+$, and $C-PyH^+$ in Figure 2 and the distances of $N-H_1$ and O_1-H_1 (R_{N-H1} and R_{O1-H1} in Table 4), it can be seen that, in the three models representing H−ZSM-5, all of the pyridine is protonated by H−ZSM-5 and the ion-pair structure of $[ZeO-PyH^+]$ is formed. With the formation of PyH^+, the acidic proton, which had been attached to the nitrogen of pyridine, has a hydrogen bond to the bridging oxygen O_1, with O_1-H_1 distances ranging from 1.474 to 2.418 Å, and the $Al-H_1$ distance is accordingly elongated by 0.106−1.439 Å. Except for the case of the intersection model of H−ZSM-5 (Figure 2, $A-PyH^+$), the structure of the zeolite framework near the acidic sites does not change significantly upon adsorption because of the weak interaction of the adsorption.

For pyridine adsorption in H−ZSM-5, it can be found that there are two kinds of interactions between the adsorbate and the substrate. In addition to the strong interaction between the acidic proton of zeolite, which has been transferred into the nitrogen of pyridine, and one of the bridging oxygen atoms bonded to Al, there are about 10 H-bond interactions between the hydrogen atoms of the CH groups in pyridine and the lattice oxygen atoms of the zeolite model, with O−H distances ranging from 2.145 to 2.936 Å (Table 4).

For the case of pyridine adsorption in Li− and Na−ZSM-5, it was found that there is a strong interaction between the pyridine nitrogen and the alkali-metal cation, with N−X distances ranging from 2.122 to 2.314 Å and 2.327 to 2.363 Å for X = Li and Na, respectively, and the N−X distance increases with increasing radii of these two cations. In all of the adsorption models, the structures of the Lewis acidic sites and pyridine molecule are almost not perturbed upon the adsorption. In Na−ZSM-5, the adsorption of pyridine is significantly weaker than that in Li−ZSM-5, according to the weaker acidity of Na^+

TABLE 5: Structural Parameters of Pyridine Adsorption Complexes in Li−ZSM-5 and Na−ZSM-5 Models[a]

	Li−ZSM-5			Na−ZSM-5		
	intersection (A−Py−Li^+)	straight channel (B−Py−Li^+)	sinusoidal channel (C−Py−Li^+)	intersection (A−Py−Na^+)	straight channel (B−Py−Na^+)	sinusoidal channel (C−Py−Na^+)
R_{Al-O1}	1.785	1.740	1.729	1.760	1.817	1.775
R_{Al-O2}	1.756	1.642	1.689	1.702	1.709	1.708
R_{Si-O1}	1.593	1.606	1.611	1.591	1.611	1.613
$\alpha_{Si-O1-Al}$	140.7	154.2	136.9	144.1	151.6	136.8
R_{X-O1}	1.897	2.002	1.892	2.861	2.334	2.296
R_{X-O2}	1.940	2.012	1.940	2.285	2.352	2.345
R_{Al-X}	2.506	2.442	2.486	3.046	2.918	2.968
R_{N-X}	2.122	2.314	2.242	2.328	2.327	2.363
R_{X-O3}				2.790		
R_{X-O4}				2.472		
R_{O3-H2} (R_{O4-H4})	2.823	2.167	2.691			(2.418)
R_{O4-H1} (R_{O4-H3})	2.981		2.641		(2.772)	2.449
R_{O5-H2} (R_{O5-H3})	2.662	2.452	2.637	2.410	2.670	2.439 (2.524)
R_{O6-H3} (R_{O6-H2})	2.646	(2.991)	2.830	2.978	2.462	2.824 (2.768)
R_{O7-H3} (R_{O7-H4})	2.806	(2.202)	2.639	(2.404)	2.467	(2.784)
R_{O7-H5}		2.766				
R_{O8-H4} (R_{O8-H2})	2.670	2.754	2.293		(2.465)	(2.818)
R_{O9-H4} (R_{O9-H2})	2.963	2.615	2.333		(2.777)	2.920
R_{O10-H5} (R_{O10-H4})	2.791	2.985	(2.559)			
R_{O11-H5} (R_{O9-H5})	2.861	(2.754)				

[a] For the numbering systems, see Figures 3 and 4.

compared to that of the Li^+ ion and reflected by a N−Na distance longer than that of N−Li. This is also reflected by the ΔE_{ads}, which is larger in Li−ZSM-5 than in Na−ZSM-5 (which will be discussed in the next section). Except for the coordination of pyridine nitrogen to the alkali cations of Li^+ and Na^+, there also exist multiple electrostatic interactions between pyridine hydrogen atoms and zeolite lattice oxygen atoms with an O−H distance smaller than 3.0 Å (Table 5). Because Li^+ and Na^+ ions are larger in size than H^+, the adsorbed pyridine in Li− and Na−ZSM-5 is farther from the adsorption site than it is in H−ZSM-5 and, thus, the oxygen atoms, which have electrostatic interactions with the pyridine hydrogen atoms, are not included in the high-level layer.

3.3. ΔE_{ads} Values of Pyridine in the Channels and the Intersection of ZSM-5. Table 2 reports the energies of pyridine adsorption in the intersection and in the two channels of ZSM-5. ΔE_{ads} is defined as the energy difference between the adsorption complex ($E_{pyridine-ZeOX}$) and the two monomers (isolated zeolite models, E_{ZeOX}, and the free pyridine molecule, $E_{pyridine}$), where X means the charge-compensating ion of H, Li, or Na.

By comparing the ΔE_{ads} values calculated from the channels and the intersections of H−, Li−, and Na−ZSM-5, it was found that the energies in the intersection region of 197.0, 172.5, and 122.3 kJ/mol are much closer to the experimental values of 200 ± 5,[31] 155−195, and 120 kJ/mol,[37] respectively, than the energies in the channels (157.9 and 127.6, 152.2 and 149.4, and 150.4 and 109.9 kJ/mol, respectively), indicating that the most probable adsorption site for pyridine in ZSM-5 is the intersection region of the straight and sinusoidal channels. Thus, one can conclude that molecules with dimensions similar or larger than those of pyridine can only be held in this region, and the active sites for most of the chemical reactions catalyzed by ZSM-5 are in the intersection region.

Except for Na−ZSM-5, the ΔE_{ads} values of pyridine calculated from the three models increase in the following order: straight channel < sinusoidal channel < intersection. In Na−ZSM-5, the energy in the sinusoidal channel is the largest one, which is due to the special location of Na^+ in the six-membered ring, which results in the reduced acidity of Na^+ in the intersection model because it was found that when Na^+ is farther from the ring, it is more acidic.[38] As for Li− and Na−ZSM-5, the energy of pyridine adsorption for the acid site in Li−ZSM-5 is larger than that for Na−ZSM-5 at the same location, which is consistent with the Lewis acidity of these two cations.

For pyridine adsorption in the intersection region of Na−ZSM-5, calculations on the **22/8T** model are also carried out. It was found that the structure of the adsorption complex is not affected by different high-layer models, while ΔE_{ads} is decreased by 10 kJ/mol in the **22/8T** model. This indicates that the inclusion of the six-membered ring in the high-layer model stabilizes the bare cluster more than the adsorption complex.

The ΔE_{ads} value of a molecule interacting with a zeolite framework is governed by two types of interactions;[38] one is the chemical interaction of the reactive part of the molecule with the active site of the zeolite (hydrogen bond, coordinative chemical bond, or electrostatic interaction), and the other is the dispersive van der Waals type of interaction of the rest of the molecule with the zeolite walls, namely, the hydrogen bonds formed between the guest molecule and the zeolite framework. For pyridine adsorption in ZSM-5, the latter part has an important contribution to ΔE_{ads}; because pyridine has a dimension similar to that of the 10-membered ring channels of ZSM-5, there will be multiple electrostatic interactions of the pyridine hydrogen atoms and the oxygen atoms of the zeolite wall.

To separate these two types of contributions, we used small clusters to exclusively estimate the first type of interactions, and it is expected that the calculated ΔE_{ads} values are lower than the experimental values. On the basis of the structural properties of the acid sites in H−, Li−, and Na−ZSM-5, 2T, 4T, and 8T clusters, which are respectively cut from the high layers of **22/2T**, **22/4T**, and **22/8T** of the intersection models of H−, Li−, and Na−ZSM-5, were used to represent the acid sites in these three zeolites. It was found that the calculated ΔE_{ads} values on these small clusters at the B3LYP/6-31G(d,p) level are only 115.0, 104.3, and 82.7 kJ/mol, respectively, which is 58% of the energy of 197.0 kJ/mol in H−ZSM-5, 60% of 172.5 kJ/mol in Li−ZSM-5, and 68% of 122.3 kJ/mol in Na−ZSM-5 calculated with **22/4T** ONIOM2 methods. On this basis, it can be roughly approximated that, in H−ZSM-5, the energy comes from the electrostatic interaction responsible for 42% of the total ΔE_{ads}, while the first part of the energy that is related

TABLE 6: Mulliken Atomic Charges on Selected Atoms of the Bare Models and Their Pyridine Adsorption Complexes in the Intersections of H−, Li−, and Na−ZSM-5[a]

	H−ZSM-5		Li−ZSM-5		Na−ZSM-5	
	bare model	adsorbed	bare model	adsorbed	bare model	adsorbed
Al	1.457	1.435	1.574	1.574	1.541	1.561
Si	1.984	1.926	1.987	1.975	1.948	1.962
X	0.519	0.508	0.480	0.357	0.462	0.208
O_1	−1.006	−1.074	−1.102	−1.080	−1.064	−1.065
O_2	−1.104	−1.090	−1.107	−1.091	−1.142	−1.125
O_3	−1.106	−1.096	−1.110	−1.112	−1.144	−1.139
H_2	0.256	0.387	0.256	0.284	0.256	0.465
H_3	0.256	0.358	0.256	0.304	0.256	0.408
H[b]	0.250	0.329	0.250	0.302	0.250	0.361
N	−0.669	−0.962	−0.669	−0.785	−0.669	−0.771

[a] For the numbering systems, see Figures 2−4. [b] The average charge on the other hydrogen atoms of pyridine.

to the Brønsted acid site only amounts to 58% of the total ΔE_{ads}. For Li− and Na−ZSM-5, the coordination of the nitrogen of the pyridine to the alkali cation is responsible for 60 and 68% of the total ΔE_{ads}, respectively, while another 40 and 32%, respectively, are due to the electrostatic interaction.

For the two channels of H−, Li−, and Na−ZSM-5, the energy decomposition calculations are also carried out on 4T clusters for comparison (Table 2). The results show that the coordination energy of pyridine nitrogen to the zeolite charge-compensating cation is responsible for 76, 70, and 72% of the total ΔE_{ads} in the straight channel and 52, 74, and 67% in the sinusoidal channel, respectively, and the rest comes from the long-range electrostatic interaction. These results show the same qualitative picture as that found in the intersection.

It is reported that, for methanol adsorbed on Na^+-exchanged zeolites, about 80% of the calculated binding energy of the guest molecule to an active site is derived from the coordination of the methanol oxygen center to the alkali cation, while only 20% is due to the electrostatic interaction.[38] For pyridine, which has a larger dimension and more hydrogen atoms than methanol, there are more hydrogen bonds that can be formed in the adsorption complexes and, thus, the contributions from electrostatic interactions to the total ΔE_{ads} are larger than those for methanol adsorption. This also indicates that the zeolite framework surrounding the acidic sites has an important effect on the adsorption of a large molecule such as pyridine. In addition, it was found that the decrease of Lewis acidity of the alkali-metal cations from Li^+ to Cs^+ can change the relative contributions of the coordination and the electrostatic interaction to the total ΔE_{ads}.[38] Our result that, in Li− and Na−ZSM-5, there are different contributions of the coordination energy and the electrostatic interaction is in agreement with this conclusion.

3.4. Electronic Properties of Pyridine Adsorption Complexes in H−, Li−, and Na−ZSM-5. The atomic charges estimated by Mulliken populations on the selected atoms of pyridine adsorption complexes in the intersection regions of H−, Li−, and Na−ZSM-5 are reported in Table 6. For comparison, the charges on these atoms in the bare models are also presented. It can be seen that the adsorption of pyridine decreases the positive charge on the compensating cations, which is reduced by 0.011−0.254 *e* as compared to the corresponding bare model. While the negative charge on the pyridine nitrogen center increases significantly after adsorption, by 0.102−0.293 *e*, the positive charges on the hydrogen atoms of the CH groups also increase. In addition to these changes, the charges on other atoms of the zeolite framework, such as Si, Al, and O, are also affected by the adsorption, while the changes occur in an unorderly way.

4. Conclusions

Pyridine adsorption in the straight and sinusoidal channels and their intersection of H−, Li−, and Na−ZSM-5 was investigated by the ONIOM2 theoretical method. It was shown that the most likely adsorption site for pyridine in ZSM-5 is the intersection of the straight and sinusoidal channels. The calculated ΔE_{ads} values of 197.0, 172.5, and 122.3 kJ/mol, respectively, in the intersections of H−, Li−, and Na−ZSM-5 are in good agreement with the experimental values of 200 ± 5, 155−195, and 120 kJ/mol. In H−ZSM-5, proton transfer from the Brønsted acidic sites to the nitrogen of the guest molecule has been found upon pyridine adsorption, while in Li− and Na−ZSM-5, the electrostatic interaction between the alkali cation and the nitrogen atoms dominates the overall interaction. In addition to this interaction, the adsorption complexes were further stabilized by long-range electrostatic interaction between the hydrogen atoms of pyridine and the lattice oxygen atoms of the zeolite framework, which is responsible for 42% of the total ΔE_{ads} in the intersection of H−ZSM-5 and 40 and 32% in the intersections of Li− and Na−ZSM-5, respectively.

Acknowledgment. The authors are grateful to the National Natural Science Foundation of China (No. 20403028), The State Key Fundamental Research Project, and the Chinese Academy of Sciences for their financial support and to the Alexander von Humboldt Foundation for the donation of computing facilities.

References and Notes

(1) Hathaway, P. E.; David, M. E. *J. Catal.* **1989**, *119*, 497.

(2) Corma, A. *Mater. Res. Soc. Symp. Proc.* **1997**, *233*, 17.

(3) Fu, Z. H.; Ono, Y. *Catal. Lett.* **1993**, *21*, 43.

(4) (a) Buzzoni, R.; Bordiga, S.; Ricchiardi, G.; Lamberti, C.; Zecchina, A. *Langmuir* **1996**, *12*, 930. (b) Meloni, D.; Laforge, S.; Martin, D.; Guisnet, M.; Rombi, E.; Solinas, V. *Appl. Catal., A* **2001**, *215*, 55.

(5) Karge, H. G.; Dondur, V.; Weitkamp, J. *J. Phys. Chem.* **1991**, *95*, 283.

(6) Defosse, G.; Canesson, P. *J. Chem. Soc., Faraday Trans. 1* **1976**, *72*, 2265.

(7) Ripmeester, J. A. *J. Am. Chem. Soc.* **1983**, *105*, 2925.

(8) (a) Zygmunt, S. A.; Curtiss, L. A.; Zapol, P.; Iton, L. E. *J. Phys. Chem. B* **2000**, *104*, 1944. (b) Brand, H. V.; Curtiss, L. A.; Iton, L. E. *J. Phys. Chem.* **1993**, *97*, 12773.

(9) Yuan, S. P.; Wang, J. G.; Li, Y. W.; Jiao, H. *J. Phys. Chem. A* **2002**, *106*, 8167.

(10) Yuan, S. P.; Wang, J. G.; Li, Y. W.; Jiao, H. *THEOCHEM* **2004**, *674*, 267.

(11) (a) Deka, R. C.; Hirao, K. *J. Mol. Catal. A* **2002**, *181*, 275. (b) Brändle, M.; Sauer, J. *J. Am. Chem. Soc.* **1998**, *120*, 1556.

(12) (a) Maseras, F.; Morokuma, K. *J. Comput. Chem.* **1995**, *16*, 1170. (b) Dapprich, S.; Komáromi, I.; Byun, K. S.; Morokuma, K.; Frisch, M. J. *THEOCHEM* **1999**, *461*, 1. (c) Tschumper, G. S.; Morokuma, K. *THEOCHEM* **2002**, *592*, 137.

(13) Vollmer, J. M.; Stefanovich, E. V.; Truong, T. N. *J. Phys. Chem. B* **1999**, *103*, 9415.

(14) Li, P.; Xiang, Y.; Grassian, V. H.; Larsen, S. C. *J. Phys. Chem. B* **1999**, *103*, 5058.

(15) Teunissen, E. H.; van Duijneveldt, F. B.; van Santen, R. A. *J. Phys. Chem.* **1992**, *96*, 366.

(16) Haase, F.; Sauer, J. *Microporous Mater.* **2000**, *35*−*36*, 379.

(17) Jobic, H.; Tuel, A.; Krossner, M.; Sauer, J. *J. Phys. Chem.* **1996**, *100*, 19545.

(18) Torrent, M.; Vreven, T.; Musaev, D. G.; Morokuma, K. *J. Am. Chem. Soc.* **2002**, *124*, 192.

(19) Tang, H.-R.; Fan, K.-N. *Chem. Phys. Lett.* **2000**, *330*, 509.

(20) Kasuriya, S.; Namuangruk, S.; Treesukol, P.; Tirtowidjojo, M.; Limtrakul, J. *J. Catal.* **2003**, *219*, 320.
(21) Roggero, I.; Civalleri, B.; Ugliengo, P. *Chem. Phys. Lett.* **2001**, *341*, 625.
(22) Solans-Monfort, X.; Bertran, J.; Branchadell, V.; Sodupe, M. *J. Phys. Chem. B* **2002**, *106*, 10220.
(23) van Koningsveld, H.; van Bekkum, H.; Jansen, J. C. *Acta Crystallogr., Sect. B* **1987**, *B43*, 127.
(24) Lonsinger, S. R.; Chakraborty, A. K.; Theodorou, D. N.; Bell, A. T. *Catal. Lett.* **1991**, *11*, 209.
(25) Sierka, M.; Sauer, J. *J. Phys. Chem. B* **2001**, *105*, 1603.
(26) Raksakoon, C.; Limtrakul, J. *THEOCHEM* **2003**, *631*, 147.
(27) *Gaussian 03*, revision B.04; Frisch, M. J., Trucks, G. W., Schlegel, H. B., Scuseria, G. E., Robb, M. A., Cheeseman, J. R., Montgomery, Jr., J. A., Vreven, T., Kudin, K. N., Burant, J. C., Millam, J. M., Iyengar, S. S., Tomasi, J., Barone, V., Mennucci, B., Cossi, M., Scalmani, G., Rega, N., Petersson, G. A., Nakatsuji, H., Hada, M., Ehara, M., Toyota, K., Fukuda, R., Hasegawa, J., Ishida, M., Nakajima, T., Honda, Y., Kitao, O., Nakai, H., Klene, M., Li, X., Knox, J. E., Hratchian, H. P., Cross, J. B., Bakken, V., Adamo, C., Jaramillo, J., Gomperts, R., Stratmann, R. E., Yazyev, O., Austin, A. J., Cammi, R., Pomelli, C., Ochterski, J. W., Ayala, P. Y., Morokuma, K., Voth, G. A., Salvador, P., Dannenberg, J. J., Zakrzewski, V. G., Dapprich, S., Daniels, A. D., Strain, M. C., Farkas, O., Malick, D. K., Rabuck, A. D., Raghavachari, K., Foresman, J. B., Ortiz, J. V., Cui, Q., Baboul, A. G., Clifford, S., Cioslowski, J., Stefanov, B. B., Liu, G., Liashenko, A., Piskorz, P., Komaromi, I., Martin, R. L., Fox, D. J., Keith, T., Al-Laham, M. A., Peng, C. Y., Nanayakkara, A., Challacombe, M., Gill, P. M. W., Johnson, B., Chen, W., Wong, M. W., Gonzalez, C., Pople, J. A, Eds.; Gaussian, Inc.: Pittsburgh, PA, 2003.
(28) Wells, D. H., Jr.; Delgass, W. N.; Thomson K. T. *J. Catal.* **2004**, *225*, 69.
(29) Fortunelli, A.; Selmi, M. *Chem. Phys. Lett*. **1994**, *223*, 390. The biggest effect found in norborane for each C−C bond is ca. 0.2 kcal/mol.
(30) Freude, D.; Klinowski, J.; Hamdan, H. *Chem. Phys. Lett.* **1988**, *149*, 355.
(31) Parrillo, D. J.; Lee, C.; Gorte, R. J.; White, D.; Farneth, W. E. *J. Phys. Chem.* **1995**, *99*, 8745.
(32) Hosono, H.; Kawazoe, H.; Nishii, J.; Kanazawa, J. *J. Non-Cryst. Solids* **1982**, *51*, 217.
(33) Bobuatong, K.; Limtrakul, J. J. *Appl. Catal., A* **2003**, *253*, 49.
(34) Deka, R. C.; Roy, R. K.; Hirao, K. *Chem. Phys. Lett.* **2000**, *332*, 576.
(35) Vayssilov, G. N.; Staufer, M.; Belling, T.; Neyman, K. M.; Knözinger, H.; Rösch, N. *J. Phys. Chem. B* **1999**, *103*, 7920.
(36) WebElements Periodic Table, Professional Edition. http://www.webelements.com.
(37) Bludau, H.; Karge, H. G.; Niessen, W. *Microporous Mater*. **1998**, *22*, 297.
(38) Vayssilov, G. N.; Lercher, J. A.; Rösch, N. *J. Phys. Chem. B* **2000**, *104*, 861.